A tailored multi-frequency EPR approach to accurately determine the magnetic resonance parameters of dynamic nuclear polarization agents: application to AMUPol

Gast, P.; Mance, D.; Zurlo, E.; Ivanov, K.L.; Baldus, M.; Huber, M.I.

PCCP

PAPER

View Article Online
View Journal | View Issue

Cite this: *Phys. Chem. Chem. Phys.*, 2017, **19**, 3777

A tailored multi-frequency EPR approach to accurately determine the magnetic resonance parameters of dynamic nuclear polarization agents: application to AMUPol†

P. Gast,[a] D. Mance,[b] E. Zurlo,[a] K. L. Ivanov,[cd] M. Baldus[b] and M. Huber*[a]

Received 24th August 2016,
Accepted 19th December 2016

DOI: 10.1039/c6cp05864g

www.rsc.org/pccp

To understand the dynamic nuclear polarization (DNP) enhancements of biradical polarizing agents, the magnetic resonance parameters need to be known. We describe a tailored EPR approach to accurately determine electron spin–spin coupling parameters using a combination of standard (9 GHz), high (95 GHz) and ultra-high (275 GHz) frequency EPR. Comparing liquid- and frozen-solution continuous-wave EPR spectra provides accurate anisotropic dipolar interaction D and isotropic exchange interaction J parameters of the DNP biradical AMUPol. We found that D was larger by as much as 30% compared to earlier estimates, and that J is 43 MHz, whereas before it was considered to be negligible. With the refined data, quantum mechanical calculations confirm that an increase in dipolar electron–electron couplings leads to higher cross-effect DNP efficiencies. Moreover, the DNP calculations qualitatively reproduce the difference of TOTAPOL and AMUPol DNP efficiencies found experimentally and suggest that AMUPol is particularly effective in improving the DNP efficiency at magnetic fields higher than 500 MHz. The multi-frequency EPR approach will aid in predicting the optimal structures for future DNP agents.

Introduction

Dynamic nuclear polarization (DNP)[1,2] has become an established method to enhance signal intensities in NMR and MRI.[3–5] For solid-state NMR (ssNMR) DNP, biradicals that follow the cross-effect (CE) polarization transfer mechanism have been proven to be advantageous to mono-radicals.[3] An important step forward in their use for applications in biosolids and materials was achieved with the design of TOTAPOL.[6] However, later work showed that TOTAPOL has a relatively flexible structure which complicates fulfilling the frequency-matching conditions required for an efficient CE mechanism.[7] In addition, recent years have shown that besides the molecular structure and rigidity, several other factors such as the electron spin relaxation times T_{1e} and T_{2e} are critical for the CE efficiency.[8–10] Hence the determination of reliable molecular parameters that determine the biradical magnetic resonance properties is critical for the design and analysis of current high-field DNP approaches. Here we show that for AMUPol[10] (Fig. 1), one of the currently most promising agents, we can determine reliable magnetic resonance parameters using a combined very high (275 GHz) and high-frequency (95 GHz) multifrequency electron paramagnetic resonance (EPR) approach

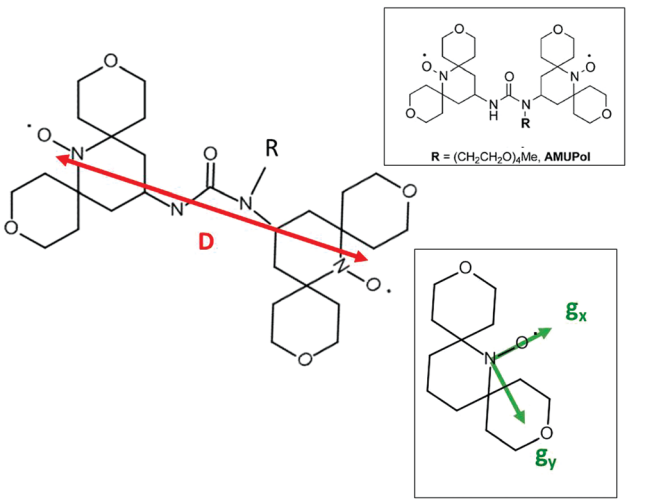

Fig. 1 Chemical structure of AMUPol, see the inset at the top, and illustration of the direction of the parallel component of the dipolar tensor (**D**), in the present work defined as D_{xx}, and the **g**-tensor axes (g_x, g_y and g_z), inset bottom.

[a] *Department of Physics, Huygens-Kamerlingh Onnes Laboratory, Leiden University, PO Box 9504, 2300 RA Leiden, The Netherlands. E-mail: Huber@physics.leidenuniv.nl*
[b] *NMR Spectroscopy, Bijvoet Center for Biomolecular Research, Utrecht University, 3584 CH, Utrecht, The Netherlands*
[c] *International Tomography Center, Siberian Branch of the Russian Academy of Science, Institutskaya 3a, Novosibirsk 630090, Russia*
[d] *Novosibirsk State University, Pirogova 2, Novosibirsk 63009, Russia*

† Electronic supplementary information (ESI) available: Materials and methods, additional EPR spectra, and full details of simulations. See DOI: 10.1039/c6cp05864g

to ensure the maximal resolution of the spectral features, leading to optimal sensitivity to the electron spin–spin coupling parameters. This method is universal, and particularly useful in cases where the dipolar interaction is too large for pulsed EPR methods that have a proven track record for determining spin–spin interactions in other systems, for example, see ref. 11 and 12.

The synthesis of AMUPol and liquid solution, 9 GHz EPR and density functional theory (DFT) results were described by Sauvee *et al.*[10] Because of its good water solubility, AMUPol has successfully been used both in the field of life science, for example to study membrane proteins[13–15] and cellular systems[16,17] and for (bio)-material science applications including ceramics,[18] organosilanes[19] and intact diatom biosilica.[20] Therefore the precise biradical magnetic resonance properties and the nitroxide–nitroxide orientation of AMUPol are of great interest. In a previous study,[21] we measured the electron–spin relaxation parameters of AMUPol and calculated DNP-enhancements based on estimated electron spin–spin coupling parameters. Here we determine these parameters experimentally, and compare them with the results of a liquid solution 9 GHz EPR study that appeared very recently.[22]

We used solution conditions that matched the solvent mixture in ssNMR–DNP experiments to ensure that the EPR parameters found are relevant for the DNP experiments (for details, see the ESI†). To determine the anisotropic dipolar interaction **D** and the isotropic exchange interaction J we conducted multi-frequency EPR experiments by comparing liquid- and frozen-solution spectra. For other DNP relevant biradicals, 9, 140 and 180 GHz EPR[7–9,23–27] studies were reported. Here, we measured experimental EPR spectra at 275 GHz on a laboratory-designed spectrometer described earlier,[28–30] and 95 GHz and 9 GHz EPR on standard instrumentation (see the ESI†). Simulations were performed using Easyspin.[31]

Materials and methods

275 GHz EPR

The 275 GHz EPR spectrum in frozen solution was measured on 7 mM AMUPol in a D_8-glycerol/D_2O/H_2O mixture with a volume ratio of 60/30/10 at a temperature of 100 K with a modulation amplitude of 0.12 mT at a modulation frequency of 1.7 kHz, with a total measurement time of 10 min. For room temperature EPR at 275 GHz, a special narrow tube with an inner diameter of 50 μm and an outer diameter of 250 μm was used for a 1 mM AMUPol solution. The temperature was 292.5 ± 0.3 K and the cryostat was purged with nitrogen gas. The modulation amplitude was 0.3 mT and the total measurement time was 1.5 h. The AMUPol spectra at this frequency were measured by cw-EPR to avoid line-shape distortion by anisotropic relaxation effects in echo detected EPR spectra.

95 GHz EPR

The spectrum at 94.0 GHz was obtained using an ELEXSYS E680 spectrometer (Bruker, Rheinstetten, Germany), with a laboratory-designed cavity on a 1 mM solution of AMUPol in the D_8-glycerol/D_2O/H_2O mixture (see above). The measurement conditions were: a temperature of 120 K, a microwave power of 0.15 μW, a modulation amplitude of 0.2 mT at a modulation frequency of 6 kHz and a total measurement time of ~180 min.

9 GHz EPR

Spectra at 9 GHz were obtained using the ELEXSYS E680 spectrometer (Bruker, Rheinstetten, Germany). For the frozen solution spectra, a rectangular cavity was used. The measurement conditions were: a temperature of 120 K and a microwave power of 16 μW. The liquid-solution spectra were obtained at 292 K using a super-high Q cavity (ER-SHQE), a microwave power of 0.8 mW, on 1 mM solutions of AMUPol. The modulation amplitude was 0.1 mT at a modulation frequency of 100 kHz; the total measurement time was 50 min for liquid and frozen-solution spectra.

Simulations of the EPR spectra

All simulations were performed with the EasySpin package[31] using the approaches and functions described in the ESI.†

Results and discussion

The frozen-solution EPR spectra (Fig. 2a–c) were recorded under the conditions used for DNP experiments, in particular, in the D_8-glycerol/D_2O/H_2O mixture typically used for DNP, and at temperatures close to the DNP temperature of 100 K. The exact parameters are specified for each spectrum in the Materials and methods section. These frozen-solution spectra show the increase in resolution upon moving from 9 to 95 and 275 GHz. Even in the 95 GHz EPR spectra (Fig. 2b) there is a partial overlap of the g_{xx} and g_{zz} features with the central g_{yy} feature, and only at 275 GHz (Fig. 2a), the ultra-high frequency we use here, all three spectral features are fully spectrally separated, making it easier to find starting parameters for the simulations and avoid ambiguities in parameter combinations. At 275 GHz, the g_{zz} feature, in which monoradical-nitroxide compounds split into three lines,[32,33] shows a more complex splitting pattern, which we attribute to the spin–spin interaction, and interpret below by spectral simulations. The AMUPol spectra have narrower bands and appear to be more structured than those of TOTAPOL at lower frequencies[7] and at 275 GHz,[21] suggesting that AMUPol has a more defined conformation than TOTAPOL.

To discriminate isotropic from anisotropic interactions, liquid-solution spectra were recorded (Fig. 2d and Fig. S1, ESI†). Reliable information on the isotropic exchange coupling J is derived from the 9 GHz EPR spectra recorded under low-viscosity conditions (Fig. 2d). Under these conditions, a nitroxide biradical with negligible J would have three equal-intensity lines, separated by the isotropic hyperfine coupling constant (A_{iso}) of the electron spin with the ^{14}N nucleus of the nitroxide. Therefore, the multiline spectrum (Fig. 2d) is direct evidence that J has a finite value, a conclusion also reached in a recent publication, showing a similar liquid solution 9 GHz EPR spectrum.[22] Similar lineshapes have been observed by Ayabe *et al.*[34] for other biradicals.

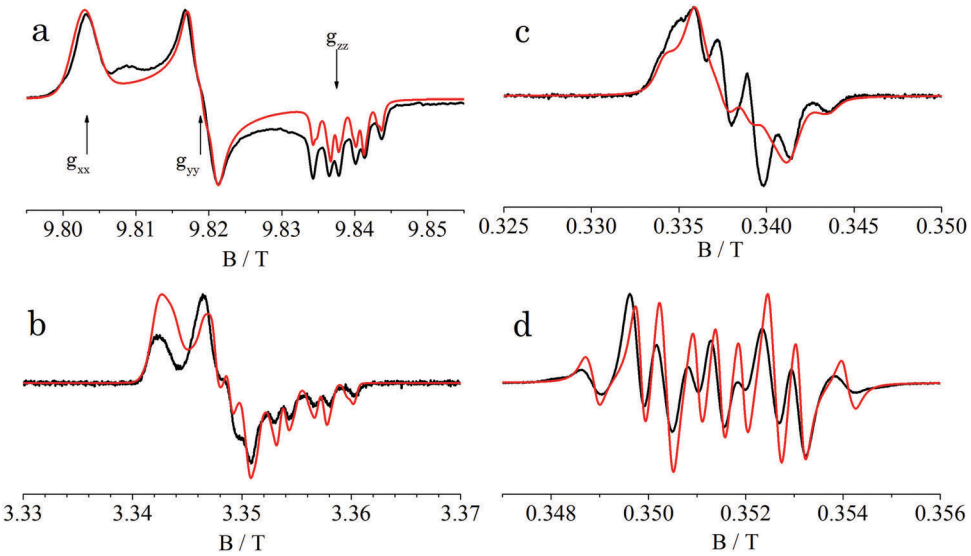

Fig. 2 Frozen solution (a–c) and room-temperature EPR (d) spectra recorded at 275, 95 and 9 GHz with simulations in red. (d) Room-temperature EPR spectrum of AMUPol at 9 GHz in water with less than 2% residual glycerol.

Simulations of the spectra shown in Fig. 2 and Fig. S1 (ESI†) were performed with one set of parameters, designed to fit the AMUPol spectra under all field/frequency and sample conditions investigated. The parameters used are described in the ESI† in detail and the **g**-, hyperfine- and dipolar tensors (**G**-, **A**-, and **D**-tensors) and exchange interaction (J) parameters are given in Table 1. Overall, the simulations fit well to the spectra (see Fig. 2 and Fig. S1, ESI†), in particular line positions and splitting patterns are well reproduced (for details, see the ESI†).

Because of the high resolution, ultra-high frequency EPR provides superior sensitivity of spectra to the **D** and **g**-tensor parameters, because all spectral features are clearly separated in the spectra (see Fig. 2a). As shown in the ESI† this also applies to the relative orientations of the tensors, which relate to the conformation of the molecule. Combining with multi-frequency EPR reduces the ambiguity in the spectral lineshape simulation. We show that according to the magnetic resonance parameters the two nitroxides of AMUPol are identical, and that the molecule has an extended conformation (see Fig. 1). Satisfactory simulations are obtained with a single conformation, in marked contrast to TOTAPOL.[6,7]

Table 1 Parameters of AMUPol obtained from the simulations of EPR spectra

	G	$A(^{14}N)$/MHz	**D**[a]/MHz	J/MHz
Measured				
xx	2.0094	27.0	−53.0	
yy	2.0061	37.0	+26.5	
zz	2.00205	94.3	+26.5	
iso	—	—	—	+43
Estimated[10,21]				
xx	2.00988	18.2	−35.0	
yy	2.00614	18.8	+17.5	
zz	2.00194	92.4	+17.5	
iso	—	—	—	0

[a] Simulations were performed with the following orientation of the **D**-tensor with respect to the **G**-tensor: the **D**-tensor unique axis (D_{par}) is rotated by 50° away from the *x*-axis of the **G**-tensor, in the *x*–*y*-plane *i.e.* towards the *y*-axis of the **G**-tensor (for details see the ESI).

Table 1 shows the simulation parameters, which are also compared to those estimated for AMUPol used previously in Mance *et al.*[21] The *D*-value is 30% larger than previously assumed. Also, an isotropic J, assumed to be negligible in our previous study and only very recently deducted from liquid-solution 9 GHz experiments,[22] is clearly seen in the data. The dipolar spin–spin interaction, **D**, from which a distance between the spins of 12.5 Å results, is in good agreement with the DFT optimized structure of AMUPol reported by Sauvee *et al.*[10] In ref. 22 two magnetic resonance parameters were determined: A_{iso}, the average of the principal components of the **A**-tensor, and the exchange interaction J. For comparison of the respective values, see the ESI.†

To assess whether the differences in magnetic resonance parameters listed in Table 1 are relevant for explaining the experimentally observed DNP enhancements, we performed simulations in the framework of the approach described in the study of Mance *et al.*,[21] where it was shown that a good agreement between DNP enhancements from simulations and experiments is obtained when relatively weak hyperfine interactions are considered. All simulations are carried out at maximum positive DNP enhancements. Similar to our previous treatment, we considered two electron spins and one spin-1/2 nucleus, but we added an additional term to the Hamiltonian reflecting the exchange coupling J between the electrons as described in the ESI.†

As before,[21] we observed a steady increase in DNP efficiency (Fig. 3a) when increasing the hyperfine interaction (HFI) from 0.023 MHz (black squares) to 3 MHz (green triangles), and the larger electron–electron coupling parameters measured in the present study by multi-frequency EPR (see Table 1) yield enhancements that are larger by 12–30% at high fields (Fig. 3a). In line with previous experimental data, we found a superior performance of AMUPol compared to TOTAPOL. To examine this aspect in

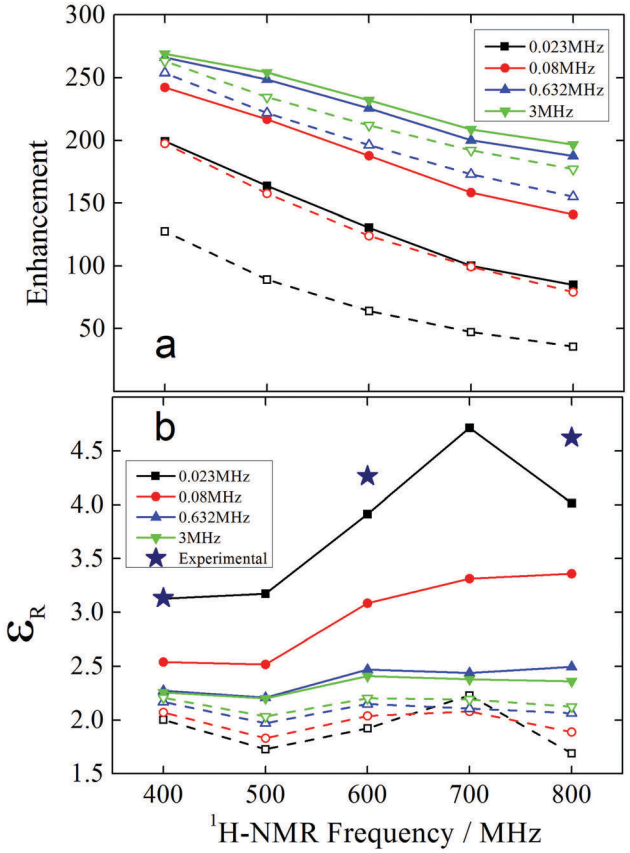

Fig. 3 Field-dependent DNP simulations for different hyperfine interactions and their comparison to experimental results, which were recorded at 8 kHz MAS at 100 K. (a) Calculated DNP enhancement factors based on estimated AMUPol parameters[10,21] (dotted lines) and AMUPol parameters measured in the current study (solid lines), for different hyperfine interactions (HFIs). (b) Calculated relative AMUPol/TOTAPOL enhancement factors ε_R using estimated (dotted lines) and experimentally determined (solid lines) spin parameters. Stars stand for measured enhancement factors that were obtained on isotope-labeled proline with a 10 mM biradical concentration. While data plotted at 400 and 600 MHz were taken from ref. 10, the data point at 800 MHz was obtained using similar experimental conditions (*i.e.* MAS rate, temperature) in the 800 MHz/527 GHz DNP setup in our own laboratory. In our simulations, 343 orientations were calculated and an MAS rate of 8 kHz was used.

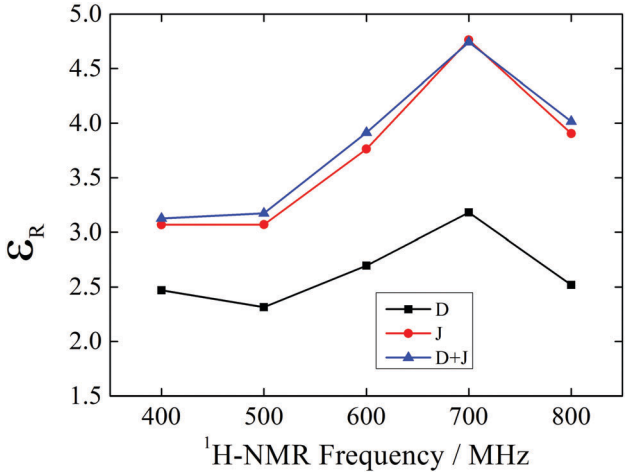

Fig. 4 Effect of biradical *J* and *D* couplings on DNP-enhancements. Calculated are the relative enhancement factors ε_R for AMUPol/TOTAPOL, using the experimentally determined spin parameters, for the case with a HFI of 0.023 MHz. The black squares represent a simulation with only the electron spin–electron spin dipole coupling *D*, the red circles show the simulation with only the exchange coupling *J* and the blue triangles show the simulation with both dipole–dipole and exchange coupling present.

further detail, we computed the relative enhancement factors $\varepsilon_R = \varepsilon(\text{AMUPol})/\varepsilon(\text{TOTAPOL})$ (Fig. 3b).

Only when using the newly determined EPR parameters (Table 1), the DNP simulations predict a significant variation in ε_R between 2.5 and 4.75 for the considered magnetic fields and hyperfine couplings, as observed experimentally (stars in Fig. 3b). In line with our previous observation,[21] a hyperfine coupling of 0.023 MHz (corresponding to an electron–nuclear distance of approx. 13 Å) best fits the experimental observations. Previous work[35,36] indicates that depolarization effects decrease at larger radical concentrations (leading to lower T_{1e} and T_{1n} values) and higher magnetic fields. Such conditions apply to our experimental DNP data and we therefore neglected depolarization effects.

Additional simulations (Fig. 4) reveal that the improved performance of AMUPol at 600 MHz and higher magnetic fields is largely due to the *J* coupling, underlining the promising potential of biradicals with sizable *J* couplings for ultra-high field DNP.[37] Further theoretical and experimental work will be needed to decide whether this observation is specific to the case of AMUPol or represents a general trend, in particular under high-field DNP conditions.

In summary, the ultra-high frequency, multi-frequency EPR approach presented here provides a powerful tool to accurately determine the parameters needed to understand and predict DNP enhancements. For AMUPol, the lineshape of EPR spectra at the three field/frequency combinations is well represented by a single conformation, in which the parallel eigenvector of the dipolar interaction tensor **D**, *i.e.* the spin–spin vector, is in the *x*–*y* plane of the nitroxides, and tilted away from the NO-bonds by 50°, towards the nitroxide *y*-tensor axis. As shown in Fig. 4, the larger electron–spin–electron–spin dipolar coupling *D* already increases DNP efficiencies, however, the dominant effect arises from the inclusion of the *J*-coupling. We find that with these novel parameters the distinct magnetic-field profile of DNP enhancement of AMUPol compared to TOTAPOL is well reproduced. The approach we present opens up a way to predict the DNP properties of molecules-to-be synthesized, thus limiting the trial and error component of DNP agent synthesis.

Conclusions

A robust set of magnetic resonance parameters of AMUPol is obtained by a multi-frequency EPR approach, which benefits particularly from the very high-field/frequency combination obtained by 275 GHz continuous wave EPR, in particular in terms of ease of determining parameters and excluding certain parameter combinations. Reliable electron–electron spin coupling parameters are derived that are relevant for the simulations of

DNP enhancements. The approach is universal and promising for a large range of DNP reagents.

Acknowledgements

We thank Prof. Alexandre Bonvin for providing access to the computational facilities at Utrecht University. This work was funded by the Netherlands Organization for Scientific Research (NWO) (Grant No. 700.26.121 and 700.10.443 to M. B. and No. 711.014.003 to M. H.) and the FOM foundation (10SMPA04 to M. H.), and supported in part by the COST Action TD-1103. K. L. I. acknowledges support from the Russian Science Foundation (Grant No. 15-13-20035). We are indebted to P. Tordo and his group for providing AMUPol.

Notes and references

1 A. W. Overhauser, *Phys. Rev.*, 1953, **92**, 411.
2 T. R. Carver and C. P. Slichter, *Phys. Rev.*, 1953, **93**, 212.
3 Q. Z. Ni, E. Daviso, T. V. Can, E. Markhasin, S. K. Jawla, T. M. Swager, R. J. Temkin, J. Herzfeld and R. G. Griffin, *Acc. Chem. Res.*, 2013, **46**, 1933.
4 J. H. Ardenkjær-Larsen, B. Fridlund, A. Gram, G. Hansson, L. Hansson, M. H. Lerche, R. Servin, M. Thaning and K. Golman, *Proc. Natl. Acad. Sci. U. S. A.*, 2003, **100**, 10158.
5 A. J. Rossini, A. Zagdoun, M. Lelli, A. Lesage, C. Copéret and L. Emsley, *Acc. Chem. Res.*, 2013, **46**, 1942.
6 C. Song, K.-N. Hu, C.-G. Joo, T. M. Swager and R. G. Griffin, *J. Am. Chem. Soc.*, 2006, **128**, 11385.
7 K.-N. Hu, C. Song, H.-H. Yu, T. M. Swager and R. G. Griffin, *J. Chem. Phys.*, 2008, **128**, 052302.
8 Y. Matsuki, T. Maly, O. Ouari, H. Karoui, F. Le Moigne, E. Rizzato, S. Lyubenova, J. Herzfeld, T. Prisner, P. Tordo and R. G. Griffin, *Angew. Chem.*, 2009, **48**, 4996.
9 A. Zagdoun, G. Casano, O. Ouari, G. Lapadula, A. J. Rossini, M. Lelli, M. Baffert, D. Gajan, L. Veyre, W. E. Maas, M. Rosay, R. T. Weber, C. Thieuleux, C. Copéret, A. Lesage, P. Tordo and L. Emsley, *J. Am. Chem. Soc.*, 2012, **134**, 2284.
10 C. Sauvee, M. Rosay, G. Casano, F. Aussenac, R. T. Weber, O. Ouari and P. Tordo, *Angew. Chem.*, 2013, **52**, 10858.
11 D. Akhmetzyanov, P. Schöps, A. Marko, N. C. Kunjir, S. T. Sigurdsson and T. F. Prisner, *Phys. Chem. Chem. Phys.*, 2015, **17**, 24446.
12 N. C. Kunjir, G. W. Reginsson, O. Schiemann and S. T. Sigurdsson, *Phys. Chem. Chem. Phys.*, 2013, **15**, 19673.
13 E. J. Koers, E. A. W. van der Cruijsen, M. Rosay, M. Weingarth, A. Prokofyev, C. Sauvee, O. Ouari, J. van der Zwan, O. Pongs, P. Tordo, W. E. Maas and M. Baldus, *J. Biomol. NMR*, 2014, **60**, 157.
14 E. A. W. van der Cruijsen, E. J. Koers, C. Sauvee, R. E. Hulse, M. Weingarth, O. Ouari, E. Perozo, P. Tordo and M. Baldus, *Chem. – Eur. J.*, 2015, **21**, 12971.
15 J. Becker-Baldus, C. Bamann, K. Saxena, H. Gustmann, L. J. Brown, R. C. D. Brown, C. Reiter, E. Bamberg, J. Wachtveitl, H. Schwalbe and C. Glaubitz, *Proc. Natl. Acad. Sci. U. S. A.*, 2015, **112**, 9896.
16 K. Yamamoto, M. A. Caporini, S.-C. Im, L. Waskell and A. Ramamoorthy, *Biochim. Biophys. Acta*, 2015, **1848**, 342.
17 M. Kaplan, A. Cukkemane, G. C. P. van Zundert, S. Narasimhan, M. Daniëls, D. Mance, G. Waksman, A. M. J. J. Bonvin, R. Fronzes, G. E. Folkers and M. Baldus, *Nat. Methods*, 2015, **12**, 649.
18 F. Blanc, L. Sperrin, D. Lee, R. Dervişoğlu, Y. Yamazaki, S. M. Haile, G. De Paëpe and C. P. Grey, *J. Phys. Chem. Lett.*, 2014, **5**, 2431.
19 D. Lee, G. Monin, N. T. Duong, I. Z. Lopez, M. Bardet, V. Mareau, L. Gonon and G. De Paëpe, *J. Am. Chem. Soc.*, 2014, **136**, 13781.
20 A. Jantschke, E. Koers, D. Mance, M. Weingarth, E. Brunner and M. Baldus, *Angew. Chem.*, 2015, **54**, 15069.
21 D. Mance, P. Gast, M. Huber, M. Baldus and K. L. T. Ivanov, *J. Chem. Phys.*, 2015, **142**, 243201.
22 C. Sauvee, G. Casano, S. Abel, A. Rockenbauer, D. Akhmetzyanov, H. Karoui, D. Siri, F. Aussenac, W. Maas, R. T. Weber, T. Prisner, M. Rosay, P. Tordo and O. Ouari, *Chem. – Eur. J.*, 2016, **22**, 5598.
23 O. Lafon, M. Rosay, F. Aussenac, X. Lu, J. Trébosc, O. Cristini, C. Kinowski, N. Touati, H. Vezin and J.-P. Amoureux, *Angew. Chem.*, 2011, **50**, 8367.
24 C. Ysacco, E. Rizzato, M.-A. Virolleaud, H. Karoui, A. Rockenbauer, F. Le Moigne, D. Siri, O. Ouari, R. G. Griffin and P. Tordo, *Phys. Chem. Chem. Phys.*, 2010, **12**, 5841.
25 W.-M. Yau, K. R. Thurber and R. Tycko, *J. Magn. Res.*, 2014, **244**, 98.
26 E. L. Dane, B. Corzilius, E. Rizzato, P. Stocker, T. Maly, A. A. Smith, R. G. Griffin, O. Ouari, P. Tordo and T. M. Swager, *J. Org. Chem.*, 2012, **77**, 1789.
27 A. Zagdoun, G. Casano, O. Ouari, M. Schwarzwälder, A. J. Rossini, F. Aussenac, M. Yulikov, G. Jeschke, C. Copéret, A. Lesage, P. Tordo and L. Emsley, *J. Am. Chem. Soc.*, 2013, **135**, 12790.
28 H. Blok, J. A. J. M. Disselhorst, S. B. Orlinskii and J. Schmidt, *J. Magn. Res.*, 2004, **166**, 92.
29 G. Mathies, H. Blok, J. Disselhorst and P. Gast, *J. Magn. Res.*, 2011, **210**, 126.
30 J. Disselhorst, H. Van der Meer and O. G. Poluektov, *J. Magn. Res.*, 1995, **115**, 183.
31 S. Stoll and A. Schweiger, *J. Magn. Res.*, 2006, **178**, 42.
32 R. Owenius, M. Engström, M. Lindgren and M. Huber, *J. Phys. Chem.*, 2001, **105**, 10967.
33 M. G. Finiguerra, H. Blok, M. Ubbink and M. Huber, *J. Magn. Res.*, 2006, **180**, 197.
34 K. Ayabe, K. Sato, S. Nishida, T. Ise, S. Nakazawa, K. Sugisaki, Y. Morita, K. Toyota, D. Shiomi, M. Kitagawa and T. Takui, *Phys. Chem. Chem. Phys.*, 2012, **14**, 9137.
35 K. R. Thurber and R. Tycko, *J. Chem. Phys.*, 2014, **140**, 184201.
36 F. Mentink-Vigier, S. Paul, D. Lee, A. Feintuch, S. Hediger, S. Vega and G. De Paëpe, *Phys. Chem. Chem. Phys.*, 2015, **17**, 21824.
37 G. Mathies, M. A. Caporini, V. K. Michaelis, Y. Liu, K.-N. Hu, D. Mance, J. L. Zweier, M. Rosay, M. Baldus and R. G. Griffin, *Angew. Chem.*, 2015, **54**, 11770.